Characterization of Radiation Loss from Microstrip Discontinuities Using a Multiport Network Modeling Approach

Albert Sabban and Kuldip C. Gupta, *Fellow, IEEE*

Abstract—**This paper presents a convenient method for evaluating radiation loss from microstrip discontinuities. The multiport network model is used to find voltage distributions around discontinuity edges, and an equivalent magnetic current model is used to compute the resulting radiation fields. As an example, the results show that for a 90° bend in a 50 Ω line on a 10-mil-thick substrate with $\epsilon_r \approx 2.2$, the radiation loss is 0.1 dB at 30 GHz. Typical power levels radiated by several other discontinuities are reported. The analysis model is verified experimentally by fabricating microstrip resonators with discontinuities incorporated therein and making measurement of Q factors of these resonators.**

I. Introduction

BECAUSE of the open nature of the microstrip configuration, hybrid and monolithic microwave circuits suffer from radiation originating at various geometrical discontinuities. Two consequences of this radiation phenomenon are additional signal loss in the circuit and undesired interactions between different parts of the circuit because of external electromagnetic coupling. These phenomena become significant in two different situations. First, when attempts are made to increase circuit density in monolithic microwave circuits, more bends and other discontinuities are introduced and spurious electromagnetic coupling increases considerably. Second, in microstrip antenna arrays, relatively thicker substrates are used and the feed network printed on the same substrate can result in substantial spurious radiation.

Estimates of the radiation loss from microstrip discontinuities have been calculated previously [1]–[6]. Most of these results are based on the Poynting vector method, developed by Lewin [1]. In this approach, a line current located at the middle of the microstrip line is taken as a source of radiation. Thus the method is applicable primarily to narrow microstrip lines. It has been applied to a 90° bend, a step discontinuity, an open end, a line terminated in an impedance, and a matched symmetrical T junction. The approach is not easily extendable to the more complicated geometries found in practical microwave circuits.

Manuscript received July 20, 1990; revised January 3, 1991. This work was supported by the NSF Industry/University Cooperative Research Center for Microwave/Millimeter-Wave Computer-Aided Design at the University of Colorado.

The authors are with the Department of Electrical and Computer Engineering, University of Colorado at Boulder, Boulder, CO 80309-0425.

IEEE Log Number 9143031.

Full-wave analysis has been used [7] to calculate radiation conductance of an open-circuited microstrip line. Full-wave analysis methods and software are available for characterization of microstrip discontinuities. These analysis include radiation effects also. The power radiated from a discontinuity may be evaluated from the computed S parameters obtained for otherwise lossless configurations (zero conductor and dielectric losses). However, evaluation of power radiated from the computed S parameters requires a high numerical accuracy of the computed results. Accurate calculation of S parameters up to the fourth decimal place require a large CPU time; therefore radiation loss values based on full-wave analysis are not widely available.

The present paper presents a convenient method for estimating radiation from microstrip discontinuities of generalized shapes. A planar multiport network model of the discontinuity configuration and the segmentation method are used to evaluate the voltage distribution around the edges of the discontinuity. This voltage distribution is expressed as an equivalent magnetic current line source distribution which is used to calculate the far-zone field (for radiation loss).

This approach is suitable for inclusion in microwave CAD packages. Numerical results have been obtained for radiation from bends, steps, and T junctions and are found to be in reasonable agreement with the Poynting vector method results wherever available.

II. Multiport Network Modeling of Microstrip Discontinuities

Multiport network modeling of microstrip discontinuity configurations [8]–[11] is based on the parallel-plate waveguide model [12] for microstrip lines. A similar network modeling approach has been used earlier for analysis of microstrip patch antennas [13] and for calculating mutual coupling between microstrip patches [14].

A. Multiport Network Model for Evaluating Edge Voltages

In order to evaluate the external fields produced by a microstrip discontinuity, we first obtain voltages at the edges of the microstrip discontinuity structure. A multiport network model similar to that developed for microstrip patch antennas [13], [14] is employed. For implementing this method, we add a number of open ports at the edges of the

0018-9480/91/0400-0705$01.00 ©1991 IEEE

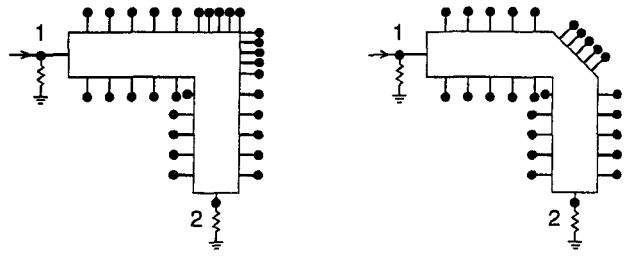

Fig. 1. Multiple ports located at the edges of the microstrip discontinuities.

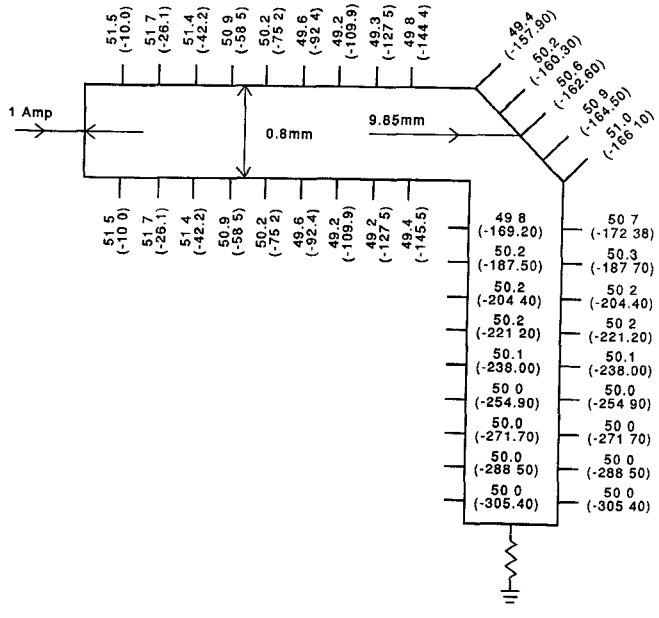

Fig. 2. Typical voltage distribution at the edges of a microstrip chamfered bend (voltage amplitude in volts, phase in degrees). $e_r = 2.2$; $h = 0.254$ mm; $Z_0 = 50\ \Omega$; $f = 10$ GHz.

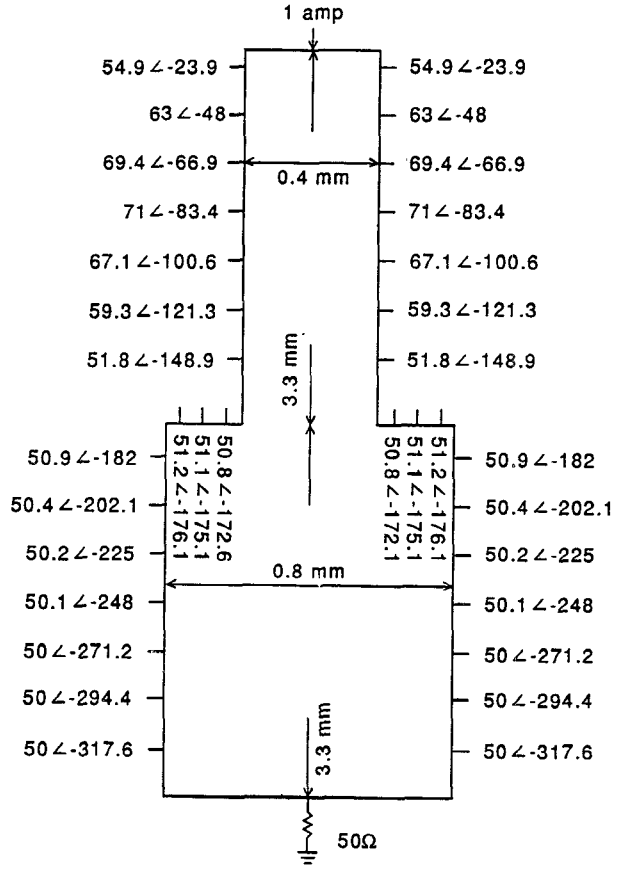

Fig. 3. Voltage distribution at the edges of a step junction when the input power is fed from a 70.7 Ω line. $e_r = 2.2$, $h = 0.254$ mm, $Z_1 = 70.7\ \Omega$, $Z_2 = 50\ \Omega$, $f = 30$ GHz. Voltage magnitude in volts, phase angle in degrees.

planar model for the discontinuity structure from which the radiation is being evaluated. This is shown in parts (a) and (b) of Fig. 1 for a right-angled bend and a compensated right-angled bend, respectively.

Lengths of transmission lines on two sides of the junction are taken large enough so that the higher order evanescent modes produced by the discontinuities are damped at the locations of external ports 1 and 2. The circuit behavior is simulated by terminating port 2 in a matched load and adding a matched source to port 1. Voltages at the N ports at the edges are computed by using the following procedure.

i) The configuration is broken down into elementary segments, connected together at the interfaces by a discrete number of interconnections.
ii) Z matrices for each of these elementary segments are evaluated by using the Green's function approach for individual geometries.
iii) Individual Z matrices obtained in (ii) are combined by using the segmentation formula.
iv) The overall multiport Z matrix is used for calculating voltages at the N edge ports for a unit current input at port 1.

Edge voltages in typical cases of a chamfered bend and step junction are shown in Figs. 2 and 3. As mentioned earlier, a somewhat similar approach has been used for designing microstrip patch antennas [13]. The only distinction in the latter case is the use of edge admittance networks (containing equivalent radiation conductances), which are connected to the edge ports. Because of the nonresonant nature of the microstrip discontinuity structures, the radiated power is small and the edge voltages may be assumed to be unaffected by the radiation conductances involved. However, when the radiated power is greater than -10 dB, radiation conductance networks are added to ports along the edges and iterative computations are carried out for evaluating voltage distributions along the edges and radiation fields.

B. Evaluation of the Radiated Power

Voltages at the discontinuity edges are represented by equivalent magnetic current sources as shown in parts (a) and (b) of Fig. 4. Each of the magnetic current line sources is divided into small sections over which the field may be assumed to be uniform. The amplitude M of each of the magnetic current elements is twice that of the edge voltage at that location, and the phase of the magnetic current is equal to the phase of the corresponding voltage. The total radiation is computed using the superposition of the far-field radiated by each section. Referring to the coordinate system, shown in Fig. 5, the far-field pattern $F(\theta, \phi)$ may be written in terms of voltages at the various elements. With the voltage

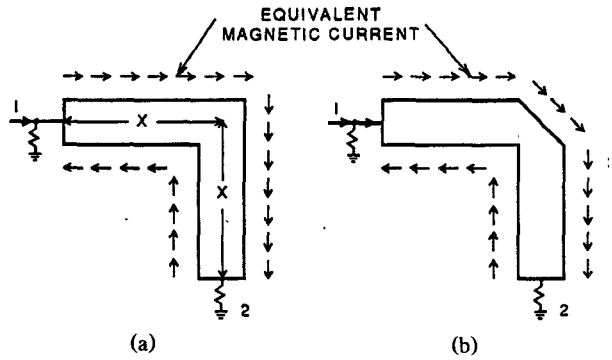

Fig. 4. Equivalent magnetic current distribution at discontinuity edges.

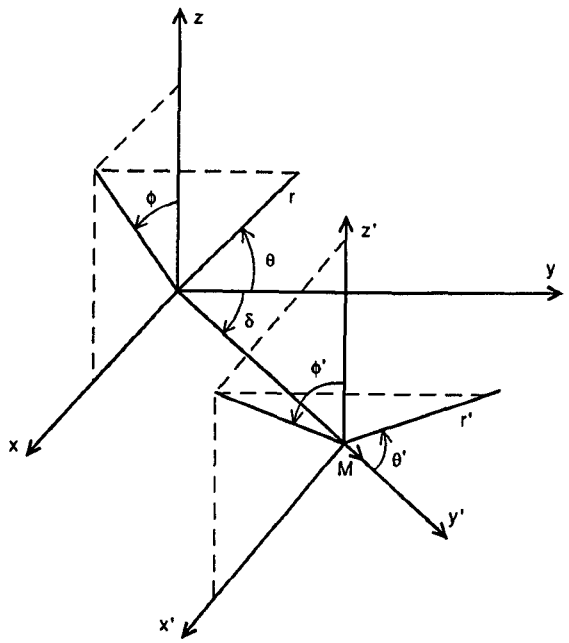

Fig. 5. Coordinate system for external field calculations.

at the ith element as $(V(i)e^{j\alpha(i)})$, we have

$$F(\theta,\phi)=\sum_{i=1}^{N}2V(i)W(i)\exp\{k_0\gamma_0(i)+\alpha(i)\}F_i(\theta,\phi) \quad (1)$$

where

$$F_i(\theta,\phi)=\frac{\sin\left(\frac{k_0W(i)}{2}\cos\theta\right)}{\frac{k_0W(i)}{2}\cos\theta}\sin\theta$$

$$\gamma_0(i)=X_0(i)\sin\theta\cos\phi+Y_0(i)\cos\theta$$

and N is the number of ports, $X_0(i)$ and $Y_0(i)$ specify the location of the ith magnetic current element, k_0 is the free space wavenumber, and $W(i)$ is the width of the ith element. The factor of 2 in (1) accounts for the image of the magnetic current with respect to the ground plane.

The radiated power is calculated by the integration of the Poynting vector over the half space and may be written as

$$P_r=\frac{1}{240\pi}\int_{-\pi/2}^{\pi/2}\int_0^{\pi}\left(|E_\theta|^2+|E_\phi|^2\right)r^2\sin\theta\,d\theta\,d\phi. \quad (2)$$

The fields E_θ and E_ϕ are expressed in terms of $F(\theta,\phi)$ as

$$E_\theta=\hat{a}_\theta\left(\frac{-jk_0}{4\pi r}F(\theta,\phi)F_\theta\right) \quad (3)$$

$$E_\phi=\hat{a}_\phi\left(\frac{-jk_0}{4\pi r}F(\theta,\phi)F_\phi\right) \quad (4)$$

where

$$F_\phi=\sin\phi'\sin\phi+\cos\delta\cos\phi\cos\phi' \quad (5)$$

$$F_\theta=-\sin\phi'\cos\theta\cos\phi+\cos\delta\cos\theta\sin\phi+\sin\delta\cos\phi'\sin\theta \quad (6)$$

and

$$\cos\theta'=\sin\theta\sin\phi\sin\delta+\cos\theta\cos\delta \quad (7)$$

$$\cos\phi'=\sin\theta\cos\phi/\sqrt{1-\cos^2\theta'}. \quad (8)$$

The radiated power may be expressed as a fraction of input power as $10\log_{10}(P_r/P_i)$ dB. The radiation loss may be expressed as

$$\text{Radiation loss (dB)}=10\log_{10}\left(1-\frac{P_r}{P_i}\right) \quad (9)$$

where P_i is the input power at port 1. P_i is calculated from input current and the input impedance of the discontinuity terminated in matched loads at other ports.

III. Computational Details

For rectangular planar segments, the single summation formulation of impedance matrix elements [15] is used. The number of terms needed for the convergence of the summation was found to be around 100.

The Z-matrix elements for sections of lossless (or low-loss) transmission line with lengths equal to multiples of a half-wavelength become infinitely large. So these line lengths should be avoided. Also, for quarter-wave sections, some of the Z-matrix elements become zero. Thus, for numerical accuracy, it is advisable to avoid quarter-wave sections also. The length of each section on either side of the discontinuity should be greater than twice the width of the microstrip line. This allows the higher order evanescent modes to be extinct at locations of the external ports (1 and 2 in Fig. 1). Also, it is found that to obtain accurate results, the width of the ports at the edges should be less than 0.075 wavelength. Computed results for different widths of interconnected ports have been studied and it is found that the optimum width of interconnected ports is about 0.05 wavelength.

In order to identify the regions of the discontinuity configuration that contribute dominantly to the radiated power, several computations were performed by taking different regions around the discontinuity. These computations show that in most of the cases the greatest contribution to the radiated power is from the ports in the region of the discontinuity itself.

IV. Numerical Results

A. Radiation from a Right-Angled Microstrip Bend

Results for the power radiated by the 90° bends (for 20 Ω and 50 Ω lines on $\epsilon_r=2.2$, $h=0.254$ mm, and for a 50 Ω bend on 127.1-μm-thick GaAs substrate) normalized with

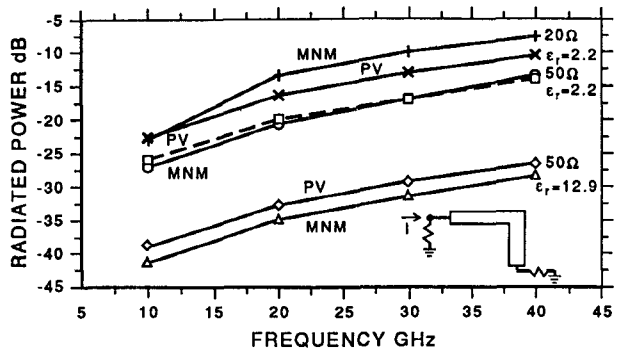

Fig. 6. Normalized radiated power from a right angled bend (MNM: multiport network model; PV: Poynting vector method [1]).

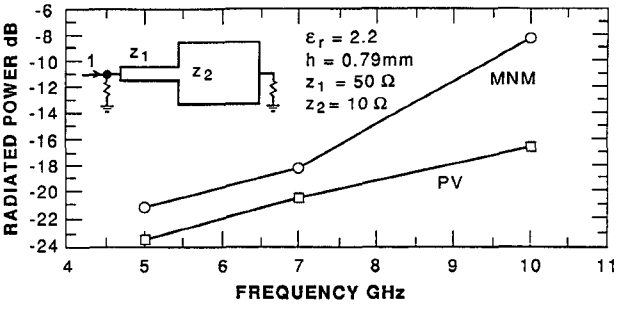

Fig. 7. Normalized radiated power from a step (MNM: multiport network model; PV: Poynting vector method [1]).

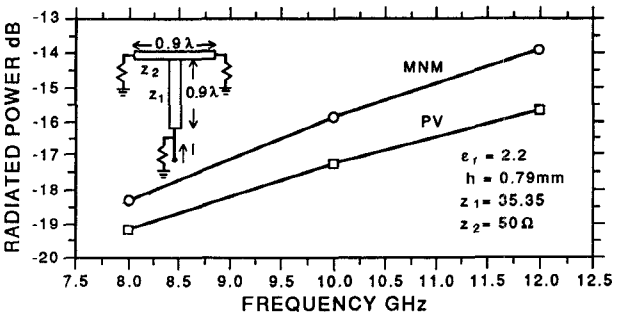

Fig. 8. Normalized radiated power from a T junction (MNM: multiport network model; PV: Poynting vector method [1]).

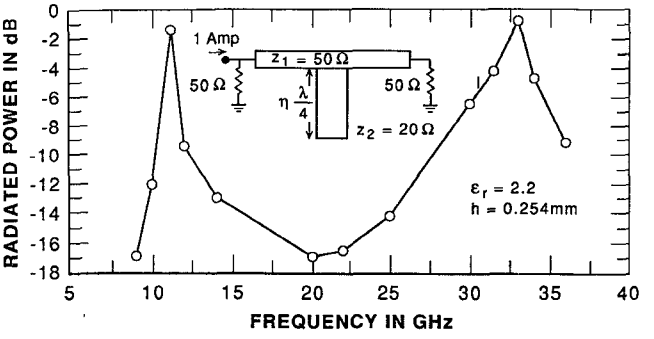

Fig. 9. Normalized radiated power from a 20 Ω open-end stub.

respect to the input power are shown in Fig. 6 for frequency ranges from 10 to 40 GHz. These results are in good agreement with results based on the complex Poynting vector method [1], which are also plotted in Fig. 6. The radiation loss at 40 GHz is 0.0062 dB for a 50 Ω line bend on a 127.1-μm-thick GaAs substrate ($\epsilon_r = 12.9$). The values for radiation loss from a 90° bend in 50 Ω line on a substrate with $\epsilon_r = 2.2$ at 30 GHz and 40 GHz are 0.1 dB and 0.17 dB, respectively. A sample check on radiation from a chamfered bend yielded radiation loss of the same order as from an uncompensated bend. These results point out that in some applications radiation from bends may need to be taken into account for accurate circuit design.

B. Radiation from a Microstrip Step Junction

Power radiated from a step junction discontinuity, with a change in impedance from 50 Ω to 10 Ω, on $\epsilon_r = 2.2$ substrate with a thickness of 0.79 mm is plotted in Fig. 7. A similar computation for a 50 Ω to 70.7 Ω junction (at 30 GHz, $\epsilon_r = 2.2$, thickness 0.254 mm) yields a normalized radiated power of −24.8 dB when the input power is fed from the 50 Ω line and −33 dB when the input is from the 70.7 Ω line. These numbers correspond to radiation loss values of 0.0143 dB and 0.00217 dB respectively. This asymmetric nature of the radiation from a step discontinuity is understandable. When the input wave is incident from the wider line, the reflection from the junction produces fringing fields similar to that at the radiating edge of a rectangular microstrip patch antenna. Hence, there is increased radiation loss in this case.

C. Radiation from a T-Junction Discontinuity

Computed results for power radiated from a T junction (50 Ω main line with a 35.35 Ω branch line on a 0.79-mm-thick substrate with $\epsilon_r = 2.2$) are shown in Fig. 8. The radiation loss for the input power incident from a branch line is 0.18 dB at 12 GHz. It is found for such a T junction that most of the contribution to the radiation losses originates from the region of the junction. Poynting vector method results are also shown in this figure. It may be noted that radiation from a T junction is also significant enough to be taken into account. This becomes very relevant when a corporate-feed arrangement is used for feeding arrays of microstrip patch antennas because a large number of power dividers employed in such situations use T junctions.

D. Radiation from a 20 Ω Open-End Stub

Power radiated from a 20 Ω stub, quarter wavelength at 10 GHz, connected to a 50 Ω line on a $\epsilon_r = 2.2$ substrate with thickness of 0.254 mm is plotted in Fig. 9. The physical length of the stub is a multiple of a quarter-wavelength at 10 GHz and at 30 GHz. Because of open-end and junction effects, the resonance frequencies are shifted to 11.3 GHz and 33 GHz respectively. The radiated power at 11.3 GHz is −1.6 dB and at 33 GHz it is −0.9 dB. Since the radiated power is high in this case, we used the iterative procedure described in subsection II-A to check the convergence of edge voltages. It may be noted that the radiation from a 20 Ω quarter-wavelength open-end stub is significant and should be taken into account in designing microstrip circuits and antennas.

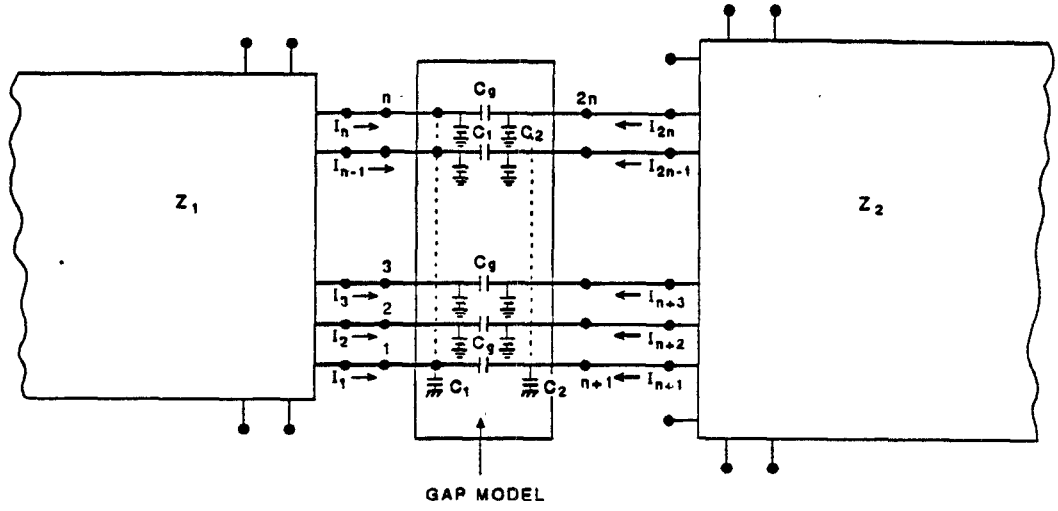

Fig. 10. Multiport network model for a gap discontinuity.

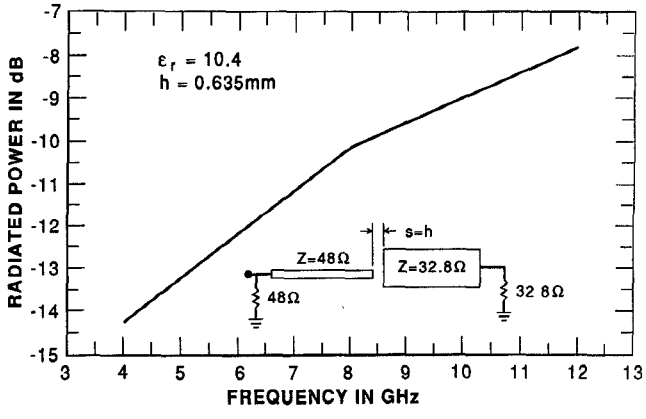

Fig. 11. Normalized radiated power from an asymmetric gap discontinuity.

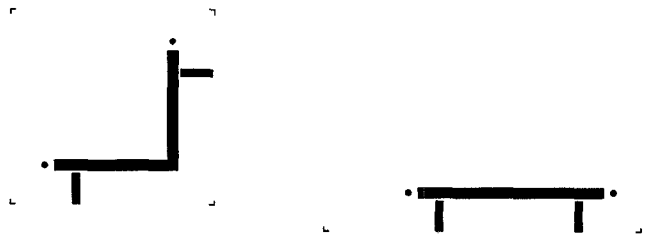

Fig. 12. (a) A bent resonator. (b) A linear resonator.

E. Radiation from a Gap

Results for power radiation from a gap discontinuity are not available in the literature. In this paper, the multiport network model is employed to evaluate radiation from gap discontinuities also. Electric field coupling in the gap region is modeled by a lumped network as shown in Fig. 10. The lumped network is derived from the capacitance matrix of the gap discontinuity. Capacitances for the gap discontinuity are obtained from equations given in [16]. One cell of the gap network section shown in Fig. 10 may be represented by the Y matrix given by.

$$[Y_C] = j\omega \begin{bmatrix} C_1 + C_g & -C_g \\ -C_g & C_2 + C_g \end{bmatrix} = j\omega [C_g]. \qquad (10)$$

For the total lumped network with n ports on each side, each for the four terms in $[C_g]$ becomes a diagonal submatrix (of size $n \times n$) with nondiagonal terms equal to zero. The corresponding impedance matrix may be written as

$$Z_G = Y_G^{-1} = \left(j\omega [C_g]\right)^{-1}. \qquad (11)$$

Power radiated from an asymmetric gap discontinuity (change in impedance from 48 Ω to 32.8 Ω, width of the gap equal to the height of the substrate 0.635 mm, $\epsilon_r = 10.4$) is plotted in Fig. 11. The radiation loss values (for input power incident from the 48 Ω line) are 0.164 dB and 0.785 dB at 4 GHz and 12 GHz, respectively. It was found that the radiation loss from an asymmetric gap and a symmetric gap are almost equal since the contribution of the magnetic current element at the edge of the input line in the gap region is dominant.

V. Experiments to Verify Radiation from Microstrip Bends

A. Design of Experiment

Since the actual radiated power levels are too small to be measured accurately, the scheme that was explored for experimental verification of radiation loss from microstrip bends consists of four gap-coupled resonant structures, similar to the two shown in parts (a) and (b) of Fig. 12. These resonators are short-circuited at the two ends so that the radiation from the open ends does not dominate the total radiation loss. The first bent resonator is approximately 2.5 wavelengths long and the bend is located at the voltage maximum. On the other hand, the second bent resonator is two wavelengths long, and a voltage null (or minimum) exists at the bend. The structure in Fig. 12(b) represents linear resonators of two-wavelengths-long and 2.5-wavelengths-long straight microstrip lines. The transmission line impedance was selected as a compromise between enhancing the radiation from the bend discontinuity and reducing the reflected power from the discontinuity. From a radiation point of view

TABLE I
COMPARISON OF MEASURED AND CALCULATED RESONANT FREQUENCIES

Resonator Type	f_r measured (GHz)	f_r calculated (GHz)	Δf (GHz)
2λ linear	9.675	9.97	0.295
2λ bent	9.91	10.1518	0.2418
2.5λ linear	9.585	9.87085	0.2858
2.5λ bent	9.635	9.8318	0.1968

a 20 Ω bend radiates more than a bend in a microstrip line with higher impedance, but computed results for S_{21} of a 20 Ω bend showed that the dip in S_{21} cannot be observed since most of the power is reflected from the bend. Comparison of computed S parameters for 20 Ω, 25 Ω, 30 Ω, 35 Ω, and 50 Ω lines indicated that an appropriate choice is 35 Ω line resonators on 0.508-mm-thick substrate with $\epsilon_r = 2.2$. Duroid, $\epsilon_r = 2.2$, has been chosen so that the radiation loss is enhanced and its measurement is simplified. In linear resonators (with the two ends shorted) the radiation losses are negligible. Thus the Q measurement on these two resonators yields conductor and dielectric losses. Values of these types of losses are accounted for while calculating the radiation loss from the measured Q factors for the bent resonators.

B. Comparison of Measured and Calculated Resonant Frequency

The resonant frequency of each resonator was calculated by detecting voltage maximum at a quarter-wavelength distance from the short-circuited ends. A comparison of the measured and computed resonant frequencies is given in Table I. The main reason for the differences between the calculated and measured resonance frequencies is the fact that the short circuits are not ideal and we have a small reactive (inductive) impedance present there. The short-circuit inductance is equivalent to an additional line length. By comparing the experimental results with calculated values for a 2λ linear resonator, we find that the value of the short-circuit inductance per unit line width is 14.57 pH/m. The value of the inductance based on measurements on the 2.5λ line resonator is found to be 17.6 pH/m.

C. Computation of Q Factors

There are three major types of losses in microstrip circuits: conductor losses, dielectric losses, and radiation losses. Losses in microstrip may also be interpreted in terms of a Q factor:

$$Q = \frac{2\pi f_r U_s}{P_l} \tag{12}$$

where U_s is the energy storage and P_l is the average power lost per unit length. The dielectric Q factor, Q_d, is inversely proportional to $\tan\delta$. The conductor loss Q factor, Q_c, is given by

$$Q_c = h\sqrt{\mu_0 \pi f_r \sigma_c} \tag{13}$$

where h is the substrate height and σ_c is the conductivity of the conductor. If we take surface roughness into account, Q_c may be approximated as $Q_c' = 0.625 Q_c$ [17]. The radiation Q factor, Q_r, is given as

$$Q_r = \frac{2\pi f_r U_s}{P_r} \tag{14}$$

where P_r is the radiated power. In all the above expressions, the energy storage, U_s, may be evaluated as

$$U_s = \frac{\epsilon_r \epsilon_0}{2h} \sum_{i=1}^{N} V^2(i)\, dx_i\, dy_i. \tag{15}$$

The resonator is divided into N cells, and $V(i)$ is the voltage at the center of the ith unit cell. The area of the ith unit cell is represented by $dx_i\, dy_i$. Usually in the discontinuity region the voltage distribution varies considerably so there are more cells in the discontinuity region. The total Q factor is

$$\frac{1}{Q} = \left(\frac{1}{Q_r} + \frac{1}{Q_c} + \frac{1}{Q_d}\right). \tag{16}$$

Since the height of the substrate is less than 0.02 wavelength, surface wave losses are negligible. The calculated Q factors for various resonators are given in Table II.

We note that in all four cases, conductor losses dominate. Radiation Q's for resonators with bends are much smaller than those for corresponding linear resonators. If we ignore radiation from the two linear resonators, the total Q values are 389.63 in both cases. The bent resonator with 2λ length has a higher total Q (348.88) than the 2.5λ resonator (300.34) and this difference is caused by lower radiation in the 2λ case (because of a voltage minimum at the bend).

D. Measurements of Q Factors

Since the calculated VSWR and the measured VSWR values were around 4:1, we employed the transmission line method to measure the Q factor. In the transmission line method, the S parameter $|S_{11}(f)|$ and $|S_{12}(f)|$ of the resonator are measured as a function of frequency, and the maximum of $|S_{12}|$ or the minimum of $|S_{11}|$ yields the resonant frequency, f_r. The loaded Q, Q_L, of the resonator is determined from the -3 dB points of $|S_{12}(f)|$:

$$Q_L = \frac{f_r}{\Delta f} \tag{17}$$

where Δf is the bandwidth at -3 dB points. The unloaded Q factor, Q, is obtained from [6]

$$Q = Q_L(1+2k) \tag{18}$$

where k is the coupling factor on both the source and load ports of the resonator. The quantity k is evaluated as [6]

$$k(f_r) = \frac{|S_{11}(f_r)|}{2|1 - S_{12}(f_r)|} \tag{19}$$

and the unloaded Q is obtained as [6]

$$Q(f_r) = \frac{Q_L(f_r)}{1 - |S_{12}(f_r)|}. \tag{20}$$

Measured resonance frequencies, values of S_{11} and S_{12} at resonance, and Δf values for the -3 dB bandwidth are used to calculate Q_L and Q, listed in Table III.

E. Computation of Radiation Q Factors

For experimental evaluation of the radiation Q associated with the bend resonators, we assume that the linear resonators have negligible radiation, and calculate other losses

TABLE II
Q FACTORS FOR THE RESONANT STRUCTURES

	2λ bent	2.5λ bent	2λ linear	2.5λ linear
f_r GHz	10.388699	9.927564	10.00009225	10.000014
P_r (W)*	180.885	175.68	123.98	72.61
Q_r	3036.08	1322.22	5884.82	6844.24
Q_d	1000	1000	1000	1000
Q_c	650.66	636.05	638.37	638.37
Q	348.88	300.34	365.44	368.65

*Normalized for an input current of 1 A.

TABLE III
MEASURED Q FACTORS

	Q_L	Q
2λ linear	169.73	198.75
2λ linear	143.62	185.04
2.5λ linear	187.94	198.25
2.5λ bent	137.64	157.75

TABLE IV
COMPARISON OF MEASURED AND CALCULATED RADIATION Q FACTORS

	2λ Bent Resonators		2.5λ Bent Resonators	
Q factor	Measured	Calculated	Measured	Calculated
Q_r	2682.47	2762.6	772.19	876.95
Q	185.04	185.25	157.75	161.9

from measured Q values. These losses are present for bent resonators also and are subtracted from the total losses for bend resonators, in order to evaluate radiation from bends. The radiation Q (thus calculated from measurements) is compared with the theoretical value based on our model.

Thus, the experimental Q_r of the bent resonators may be written as

$$\frac{1}{Q_r} = \frac{1}{Q_{\text{measured}}} - \frac{1}{Q_{\text{losses}}} \tag{21}$$

where Q_{losses} is the measured Q factor for 2λ and 2.5λ linear resonators, and Q_{measured} is the measured Q of bent resonators. Comparison between the measured and calculated radiation Q factors is given in Table IV.

In the second row of Table IV, measured values are the unloaded Q values shown in Table III, and the calculated values are based on radiation losses calculated from our model and the other losses (conductor plus dielectric, etc.) obtained from measurements on linear resonators.

The disagreement between the measured and calculated Q_r for the 2λ bent resonator is 3%, and for 2.5λ bent resonators the corresponding value is 11%. The corresponding differences for total Q are only 0.1% and 2.56% respectively. Keeping in mind the experimental uncertainties and the assumption that the conductor losses are equal in the straight and bent resonators, the agreement between theory and experiments is reasonable. This verifies the equivalent magnetic current modeling approach used for estimating radiation from microstrip discontinuities.

VI. CONCLUDING REMARKS

A convenient and versatile method (based on the multiport network modeling approach) for evaluating radiation loss associated with discontinuities in microstrip circuits has been presented in this paper. The results are in good agreement with the Poynting vector method applicable for simple geometries.

Sample reuslts presented show that radiation losses from microstrip discontinuities cannot be neglected at higher frequencies. For a 10 Ω to 50 Ω change ($\epsilon_r = 2.2$, $h = 0.79$ mm) in width, the radiation loss at 10 GHz is 0.7 dB. For a 90° bend in 50 Ω line on a 0.254-mm-thick substrate with $\epsilon_r = 2.2$, the radiation loss at 40 GHz is 0.17 dB. The multiport network model can be used for calculating radiation from complicated discontinuity configurations such as chamfered bends, compensated T junctions, and cross junctions.

Radiation Q factors obtained from measurements in resonators incorporating a right-angle bend show a fair agreement with the estimated values. This provides an experimental verification of the proposed method.

REFERENCES

[1] L. Lewin, "Radiation from discontinuities in strip-line," *Proc. Inst. Elec. Eng.*, vol. 117, pt. C, pp. 163–170, Sept. 1960.

[2] L. Lewin, "Suprious radiation from a microstrip Y-junction," *IEEE Trans. Microwave Theory Tech.*, vol. MTT-26, pp. 893–894, Nov. 1978.

[3] L. Lewin, "Spurious radiation from microstrip," *Proc. Inst. Elec. Eng.*, vol. 125, pp. 633–642, July 1978.

[4] M. D. Abouzahra and L. Lewin, "Radiation from microstrip discontinuities," *IEEE Trans. Microwave Theory Tech.*, vol. MTT-27, pp. 722–723, Aug. 1979.

[5] M. D. Abouzahra, "On the radiation from microstrip discontinuities," *IEEE Trans. Microwave Theory Tech.*, vol. MTT-29, pp. 666–668, July 1981.

[6] R. H. Hoffman, "Radiation from microstrip circuits," in *Handbook of Microwave Integrated Circuits*. Norwood, MA: Artech House, 1987, ch. 11, pp. 311–321, 205–210.

[7] P. B. Kathei and N. G. Alexopoulos, "Frequency-dependent characteristic of microstrip discontinuities in millimeter-wave integrated circuits," *IEEE Trans. Microwave Theory Tech.*, vol. MTT-33, pp. 1029–1035, Oct. 1985.

[8] I. Wolff *et al.*, "Calculation method for microstrip discontinuities and T-junctions," *Electron. Lett.*, vol. 8, pp. 177–179, 1972.

[9] W. Menzel and I. Wolff, "A method for calculating the frequency dependent properties of microstrip discontinuities," *IEEE Trans. Microwave Theory Tech.*, vol. MTT-25, pp. 107–112, 1977.

[10] R. Chadha and K. C. Gupta, "Compensation of discontinuities in planar transmission lines," *IEEE Trans. Microwave Theory Tech.*, vol. MTT-30, pp. 2151–2156, Dec. 1982.

[11] H. J. Maramis and K. C. Gupta, "Planar analysis and optimization of microstrip discontinuities," Sci. Rep. No. 96, Electromagnetics Laboratory, University of Colorado, Boulder, Mar. 1988.

[12] G. Kompa and R. Mehran, "Planar waveguide model for computing microstrip components," *Electron. Lett.*, vol. 11, no. 9, pp. 459–460, 1975.

[13] A. Benalla and K. C. Gupta, "Multiport network model and transmission characteristics of two port rectangular microstrip antennas," *IEEE Trans. Antennas Propagat.*, vol. 36, pp. 1337–1342, Oct. 1988.
[14] A. Benalla and K. C. Gupta, "Multiport network approach for modeling the mutual coupling effects in microstrip patch antennas and arrays," *IEEE Trans. Antennas Propagat.*, vol. 37, pp. 148–152, Feb. 1989.
[15] A. Benalla and K. C. Gupta, "Faster computation of Z-matrices for rectangular segments in planar microwave circuits," *IEEE Trans. Microwave Theory Tech.*, vol. MTT-35, pp. 733–736, June 1986.
[16] M. Kirschning, R. H. Jansen, and N. H. L. Koster, "Measurement and computer-aided modeling of microstrip discontinuities by an improved resonator method," in *1983 IEEE MTT-S Int. Microwave Symp. Dig.*, pp. 495–497.
[17] T. C. Edwards, *Foundations for Microstrip Circuit Design*. New York: Wiley, 1981, pp. 89–92.
[18] A. Sabban and K. C. Gupta, "Multiport network model for evaluating radiation loss and spurious coupling between discontinuities in microstrip circuits," in *1989 IEEE MTT-S Int. Microwave Symp. Dig.*, pp. 707–710.

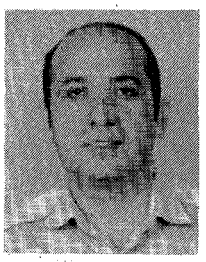

Albert Sabban received the B.Sc and M.Sc degrees in electrical engineering from Tel-Aviv University, Tel-Aviv, Israel, in 1976 and 1986, respectively.

In 1976 he joined the armament development authority, RAFAEL, where he serves as a senior Antenna and Microwave Engineer and Project Supervisor. From 1984 to 1987 he was a leader of an antenna group in RAFAEL. He is now on a leave from RAFAEL. He joined the University of Colorado, Boulder, in 1987 as a research assistant, where he is working on multiport network modeling for evaluating radiation loss and spurious coupling between discontinuities in microstrip circuits. He completed work toward the Ph.D. degree in electrical engineering at the University of Colorado in January 1991.

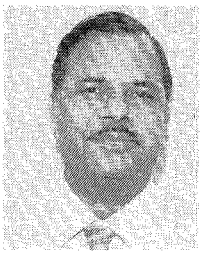

Kuldip C. Gupta (M'62–SM'74–F'88) received the B.S. and M.S. degrees in electrical communication engineering from the Indian Institute of Science, Bangalore, India, in 1961 and 1962, respectively, and the Ph.D. degree from the Birla Institute of Technology and Science, Pilani, India, in 1969.

Dr. Gupta has been at the University of Colorado since 1983, initially as a Visiting Professor and later as a Professor. Earlier, he had a long stay (beginning in 1969) at the Indian Institute of Technology, Kanpur, where he had been a Professor of Electrical Engineering Engineering since 1975. On leave from IITK, he has been a Visiting Professor at the University of Waterloo, Canada; at the Ecole Polytechnique Federale de Lausanne, Switzerland; at the Technical University of Denmark (Lyngby); at the Eidgenossische Technische Hochschule, Zurich; and at the University of Kansas, Lawrence. From 1971 to 1979 he was the Coordinator for the Phased Array Radar Group of the Advanced Center for Electronics Systems at the Indian Institute of Technology.

Dr. Gupta's current research interests are in the area of computer-aided design techniques for microwave and millimeter-wave integrated circuits and integrated antennas. He is author or coauthor of five books: *Microwave Integrated Circuits* (Wiley Eastern, 1974; Halsted Press of John Wiley, 1974), *Microstrip Lines and Slotlines* (Artech House, 1979), *Microwaves* (Wiley Eastern 1979; Halsted Press of John Wiley, 1980; Editorial Limusa Mexico, 1983), *CAD of Microwave Circuits* (Artech House, 1981; Chinese Scientific Press, 1986; Radio i Syvaz, 1987) and *Microstrip Antenna Design* (Artech House, 1988). Also, he has contributed chapters to the *Handbook of Microstrip Antennas* (Peter Peregrinus, 1989), the *Handbook of Microwave and Optical Components* (John Wiley), *Microwave Solid State Circuit Design* (John Wiley, 1988), and *Numerical Techniques for Microwave and Millimeter Wave Passive Structures* (John Wiley, 1989). Dr. Gupta has published over 130 research papers and holds two patents in the microwave area.

Dr. Gupta is a Fellow of the Institution of Electronics and Telecommunication Engineers (India). He is on the MTT-S Technical Committees on CAD (MTT-1) and Microwave Field Theory (MTT-15), and on the Technical Program Committee for MTT-S International Symposia. He is on the editorial boards of the IEEE TRANSACTIONS ON MICROWAVE THEORY AND TECHNIQUES, of *Microwave & Optical Technology Letters* (John Wiley), and of three journals of IETE (India). He is the founding editor for *International Journal of Microwave and Millimeter-wave Computer Aided Engineering*, published by John Wiley. He is listed in *Who's Who in America*.